ELSEVIER

Earth and Planetary Science Letters 153 (1997) 133–147

EPSL

Kinetics of the coesite to quartz transformation

J.L. Mosenfelder [a,*], S.R. Bohlen [b]

[a] *Department of Geological and Environmental Sciences, Stanford University, Stanford, CA 94305-2115, USA*
[b] *U.S. Geological Survey, MS-910, 345 Middlefield Road, Menlo Park, CA 94025, USA*

Received 13 March 1997; revised 18 July 1997; accepted 5 September 1997

Abstract

The survival of coesite in ultrahigh-pressure (UHP) rocks has important implications for the exhumation of subducted crustal rocks. We have conducted experiments to study the mechanism and rate of the coesite → quartz transformation using polycrystalline coesite aggregates, fabricated by devitrifying silica glass cylinders containing 2850 H/10^6 Si at 1000°C and 3.6 GPa for 24 h. Conditions were adjusted following synthesis to transform the samples at 700–1000°C at pressures 190–410 MPa below the quartz–coesite equilibrium boundary. Reaction proceeds via grain-boundary nucleation and interface-controlled growth, with characteristic reaction textures remarkably similar to those seen in natural UHP rocks. We infer that the experimental reaction mechanism is identical to that in nature, a prerequisite for reliable extrapolation of the rate data. Growth rates obtained by direct measurement differ by up to two orders of magnitude from those estimated by fitting a rate equation to the transformation–time data. Fitting the rates to Turnbull's equation for growth therefore yields two distinct sets of parameters with similar activation energies (242 or 269 kJ/mol) but significantly different pre-exponential constants. Extrapolation based on either set of growth rates suggests that coesite should not be preserved on geologic time scales if it reaches the quartz stability field at temperatures above 375–400°C. The survival of coesite has previously been linked to its inclusion in strong phases, such as garnet, that can sustain a high internal pressure during decompression. Other factors that may play a crucial role in preservation are low fluid availability — possibly even less than that of our nominally ''dry'' experiments — and the development of transformation stress, which inhibits nucleation and growth. These issues are discussed in the context of our experiments as well as recent observations from natural rocks. © 1997 Elsevier Science B.V.

Keywords: coesite; quartz; kinetics; phase transitions; high pressure

1. Introduction

Findings of coesite and diamond included in other phases in regionally metamorphosed rocks have demonstrated that significant portions of continental crust have been subducted to extreme depths (≥ 100 km) and returned to the surface [1]. Tantalizing evidence from the Alpe Arami massif [2] now suggests that some continental crust may have been subducted to and exhumed from even greater depths (≥ 300 km). These discoveries have important implications for orogeny and plate tectonics. Despite a wealth of research, however, the tectonic processes responsible for exhumation of these deep-seated rocks are still incompletely understood, and several competing tectonic models remain extant [3–5].

* Corresponding author. Bayerisches Geoinstitut, Universität Bayreuth, D-95440, Bayreuth, Germany. E-mail: jed.mosenfelder@uni-bayreuth.de

PII S0012-821X(97)00159-3

Models for exhumation must account for the partial preservation of coesite. The most commonly cited explanation for preservation is that the including phase acts as a ''pressure vessel'', inhibiting transformation to quartz by maintaining a higher internal pressure on the inclusion, until fracture of the host phase at low temperature allows reaction [6,7]. The host phase might equally well prevent the ingress of fluids to flux the transformation, but the relative importance of these two processes has not been ascertained. In order to address this question, data on the kinetics of the reaction are needed. Accordingly, we have conducted systematic experiments to determine the rate and mechanism of the transformation as a function of pressure, temperature, and time, at a fixed grain size and fluid content. Ultimately, kinetic data can be used to constrain the range of P–T–t paths that allow the preservation of coesite, providing a complementary approach to conventional methods of studying the timing and nature of exhumation, such as thermobarometry, radiometric dating, and structural geology [8,9].

2. Experimental and analytical methods

2.1. Starting material

The starting material for each experiment was a polycrystalline coesite aggregate, fabricated by devitrifying a cylinder of Corning grade G silica glass (5.4 mm in diameter by 3 mm long) at 3.6 GPa and 1000°C for 24 h in a piston–cylinder apparatus [10]. This method for synthesizing ''rocks'' leads to low porosity and moderate defect density, characteristics that are essential if the results are to be applied to model the transformation as it occurs in nature [11]. According to the manufacturer's specifications, the glass contains < 150 ppb of any contaminant with the exception of hydroxyl, with an average total impurity content of ~ 250 ppb. Water contents of the glass and the synthetic coesite were measured by FTIR using a Nicolet 550 Magna-IR spectrometer with IR microscope. The OH content of the starting glass (2850 ± 40 H/10^6 Si) was obtained from the height of the 3670 cm^{-1} peak, using an absorption coefficient of 181 l/mol [12]. The accuracy of this measurement is $\pm 4\%$ [12]. Spectra for coesite were dominated by a broad band centered around 3400 cm^{-1}, indicating that most of the hydrogen was incorporated in fluid inclusions. A total of 13 measurements on coesite yielded an average fluid content of 294 ± 111 H/10^6 Si, calculated using the calibration of Paterson [13]. Comparison of this concentration with that of the starting glass suggests that a large percentage of the initial fluid was present along grain boundaries and/or escaped from the sample. At present we have no definitive way of determining how much H_2O escaped from the capsule. Indirect evidence for a grain boundary fluid phase is provided by SEM textural observations of quartzites, synthesized using a similar method, which show pore morphologies indicative of a H_2O-rich fluid phase [10].

The aggregates consisted of tabular coesite crystals 100–200 μm long by 20–80 μm wide (Fig. 1), with an average mean linear intercept of 43 ± 6 μm. For the purpose of analyzing the rate data, we converted the intercept to an average grain size using a geometric factor of 1.5, suitable for a hexagonal prismatic crystal shape [14]. Optical and transmission electron microscopy (TEM) showed no evidence for residual glass. A moderate density of dislocations, stacking faults and twins were observed with TEM; grain boundaries were generally straight or slightly curved. Repeated syntheses as well as experiments with only small amounts of transformation confirmed that there was no significant variation in grain size or texture in different experiments.

Fig. 1. Coesite starting material, crystallized from silica glass cylinder at 1000°C, 3.6 GPa, for 24 h. *Scale bar* = 100 μm. Crossed polarized light.

2.2. Experimental procedure

The glass cylinders were encapsulated in graphite and placed into 1.91 cm NaCl furnace assemblies (Fig. 2), which were then vacuum dried at 180°C for at least 24 h in order to remove adsorbed water. The assemblies were coated with dry MoS_2 and wrapped in lead foil to reduce friction. Standard ''hot piston-in'' technique [15] was used to achieve initial P–T conditions. Temperature was measured with Pt_{100}–$Pt_{90}Rh_{10}$ thermocouples, precise to ± 5°C. No correction was made for the effect of pressure and temperature gradients on EMF. The temperature gradient, calibrated with double thermocouple experiments, was ~ 10°C/mm near the hot spot of the furnace. As a result of thermal expansion of the bottom NaCl piece (Fig. 2), the sample may have migrated up to 2 mm from the hot spot during some experiments. We estimate a maximum temperature gradient of 50°C across the sample.

After synthesis, P–T conditions were changed to those of the stability field of quartz to induce transformation (Fig. 3). Temperature was lowered at 5°C/min, followed by decompression at 10–20 MPa/min. This approach to the final conditions resulted in a ''piston-out'' condition. The slow cooling and decompression procedure was optimized to minimize cracking of the samples [16] while preventing transformation during the adjustment stage. Cracking was also reduced by the use of graphite capsules, which absorb a large component of the stress caused by decompression because of the anomalously high rate of strain recovery of graphite [17,18]. Tingle [18] used graphite to recover olivine single crystals intact from high-pressure experiments. We have also retrieved polycrystalline quartz and coesite samples without visible fractures, although some opening along grain boundaries may have occurred. Minimization of cracking is important because cracks can dictate reaction rate and mechanism by providing high-energy sites for nucleation and growth and faster pathways for diffusion.

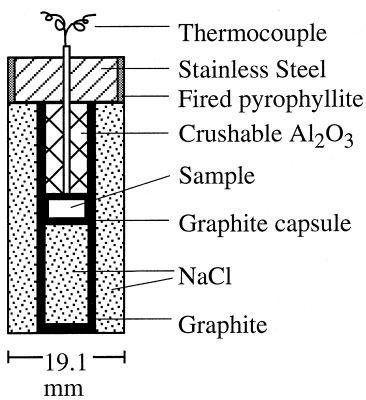

Fig. 2. Schematic view of pressure cell, similar to those used in [15,19]. No hydrous parts are used in the assembly.

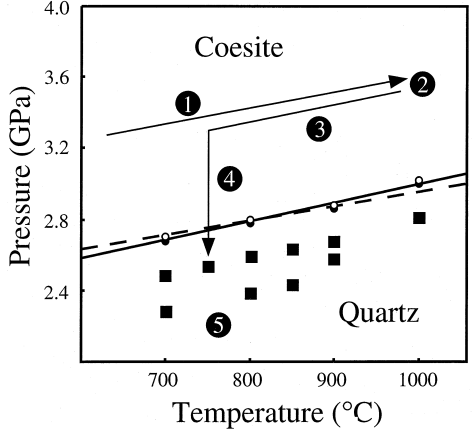

Fig. 3. Experimental P–T conditions (*squares*) and representative P–T–t path illustrating experimental methodology. *Numbers* refer to the following steps: piston-in approach (1) to synthesis (2) at 1000°C, 3.6 GPa, for 24 h; temperature decrease (3) at 5°C/min followed by decompression (4) under ''piston-out'' conditions at 10–20 MPa/min to the transformation condition (5). Calibration of the coesite ⇌ quartz equilibrium boundary for the press used [19] is shown by *black* and *white circles*. Also shown are the fit to the reversal data (*solid line*) and the calibration of Bohlen and Boettcher [41] (*dashed line*) for reference.

Experiments (Table 1) were conducted for periods up to 360 h at 700–1000°C and pressures 190–410 MPa below the equilibrium value, which was calibrated directly for the single press used for the study (Fig. 3; [19]). Uncertainty in the location of the quartz–coesite equilibrium [19,20] does not present a significant problem for this study because the main parameter of interest is not the actual pressure but $\Delta P \Delta V$, which largely determines ΔG_{rxn}. However, a potentially serious uncertainty results from the two-stage experimental procedure employed in this study, because pressure hysteresis induced by friction in the

Table 1
Experimental conditions and results

No.	T (°C)	P [a] (GPa)	P_{und} [a] (GPa)	Duration (h)	Decompression rate (MPa/min)	$\%\xi$	Growth distance (μm)	Growth rate (m s^{-1})
434	700	2.48	0.20	288	18.1	10.0	4.5	4.34×10^{-12}
362	700	2.48	0.20	360	11.0	18.3	12.5	9.65×10^{-12}
387	700	2.28	0.40	240	15.6	29.9	6.25	7.23×10^{-12}
365	750	2.53	0.21	149	12.6	26.7	16.3	3.03×10^{-11}
425	800	2.59	0.20	96	17.2	25.5	14.5	4.20×10^{-11}
433	800	2.59	0.20	120	16.0	27.3	12.0	2.78×10^{-11}
293	800	2.59	0.20	144	13.9	30.6	15.0	2.89×10^{-11}
310	800	2.59	0.20	192	10.4	45.8	27.5	3.98×10^{-11}
313	800	2.59	0.20	240	10.5	78.5	n.d.	n.d.
371	800	2.38	0.41	21.5	13.9	36.5	15.0	1.94×10^{-10}
376	800	2.38	0.41	72	16.4	49.4	18.8	7.23×10^{-11}
369	800	2.38	0.41	96	16.8	62.3	15.0	4.34×10^{-11}
379	800	2.38	0.41	120	20.7	64.5	17.5	4.05×10^{-11}
395	800	2.38	0.41	336	18.8	81	n.d.	n.d.
355	850	2.63	0.21	24	10.3	23.7	8.75	1.01×10^{-10}
363	850	2.63	0.21	36	10.7	42.4	18.8	1.45×10^{-10}
348	850	2.63	0.21	48	16.3	52.8	13.8	7.96×10^{-11}
352	850	2.63	0.21	72	13.1	52.4	26.3	1.01×10^{-10}
361	850	2.63	0.21	82	11.8	57.1	30.0	1.02×10^{-10}
357	850	2.63	0.21	96	12.8	64.5	26.3	7.60×10^{-11}
364	850	2.63	0.21	120	10.5	64.5	25.0	5.79×10^{-11}
401	850	2.43	0.41	72	16.3	64.7	17.5	6.75×10^{-11}
382	850	2.43	0.41	144	15.6	82.2	n.d.	n.d.
408	850	2.43	0.41	168	15.3	80.6	n.d.	n.d.
422	900	2.67	0.22	2	14.0	26.4	12.0	1.67×10^{-9}
428	900	2.67	0.22	6	15.6	52.3	19.0	8.80×10^{-10}
431	900	2.67	0.22	12	14.2	69.9	n.d.	n.d.
334	900	2.67	0.22	24	11.6	74.2	n.d.	n.d.
294	900	2.67	0.22	43	15.6	75.2	n.d.	n.d.
319	900	2.67	0.22	48	11.9	82.2	n.d.	n.d.
289	900	2.67	0.22	72	11.6	68.2	n.d.	n.d.
296	900	2.67	0.22	120	10.9	87.8	n.d.	n.d.
302	900	2.67	0.22	144	12.4	100	n.d.	n.d.
291	900	2.57	0.32	72	11.6	99.2	n.d.	n.d.
420	950	2.73	0.21	12	16.8	76.2	n.d.	n.d.
359	950	2.73	0.21	24	12.5	88.7	n.d.	n.d.
346	1000	2.81	0.19	0.5	13.5	29.9	25.0	1.39×10^{-8}
342	1000	2.81	0.19	4	13.9	55.6	13.8	9.55×10^{-10}
321	1000	2.81	0.19	6	14.8	72.7	n.d.	n.d.
340	1000	2.81	0.19	9	12.0	96.2	n.d.	n.d.
298	1000	2.81	0.19	20	10.8	100	n.d.	n.d.

n.d. = not determined.
[a] Pressures reported as nominal (gauge) value; P_{und} is understep from equilibrium value calibrated for the press.

apparatus is significantly greater during ''piston-out'' experiments [20,21]. The effect of this hysteresis in our apparatus has not been calibrated, and non-systematic errors could conceivably be introduced by small differences in the rate of decompression, trace concentrations of H_2O in the pressure medium [22], or the condition of the cylinder bore [21]. As a result of these combined uncertainties, we estimate the accuracy in pressure *relative to the equilibrium boundary* to be ± 0.05 GPa.

At the end of each experiment, temperature was quenched rapidly by cutting power to the furnace,

and a thin section was made of the sample for examination by optical microscopy and measurement of reaction progress (ξ) and growth rate.

2.3. Analysis of transformed samples

Optical microscopy was used to examine reaction textures and measure growth rates. Reaction progress was measured by using back-scattered electron (BSE) imaging to determine the modal proportions of quartz and coesite (Table 1). The density contrast between the two phases results in a small but detectable difference in the BSE coefficient, providing sufficient contrast for quantitative analysis (Fig. 4). Images were acquired by averaging 15 scans per pixel on a JEOL-JXA-733 Superprobe with a solid-state BSE detector and high-gain amplifier. The gain of the detector was maximized with beam voltage and current set at 15 keV and $\sim$23 nA, respectively. For each experiment, 10–12 images were acquired in a line across the width of the sample, beginning $\sim$300 μm from the top and side edges at the end closest to the thermocouple. This procedure was employed in order to avoid edge effects and the effect of the temperature gradient. Using the public-domain program NIH Image, the images were filtered to reduce random and periodic noise and then subjected to particle analysis after setting an appropriate threshold value according to the pixel intensities of quartz and coesite, taking into account the percentage of cracks in the sample. The precision of the imaging technique ($\pm$5 percentage points) was assessed by repeat processing, varying the threshold pixel intensity for phase identification.

BSE imaging overcomes several disadvantages of X-ray diffraction (XRD) and optical point counting, methods more commonly used to measure ξ. For example, powdering of samples for XRD precludes the detection of spatial variations that commonly occur as a result of temperature gradients or enhanced reaction at the capsule edge. Optical point counting may suffer from significant errors due to human bias, incorrect phase assignment due to through-focusing, and sampling errors, particularly when the grain size is small relative to the thickness of the thin section. The high spatial resolution ($\sim$1 μm) but restricted depth resolution ($\sim$2 μm) of the imaging technique eliminates these problems. Thus, while the precision of the technique is comparable to other methods, the accuracy is probably significantly better.

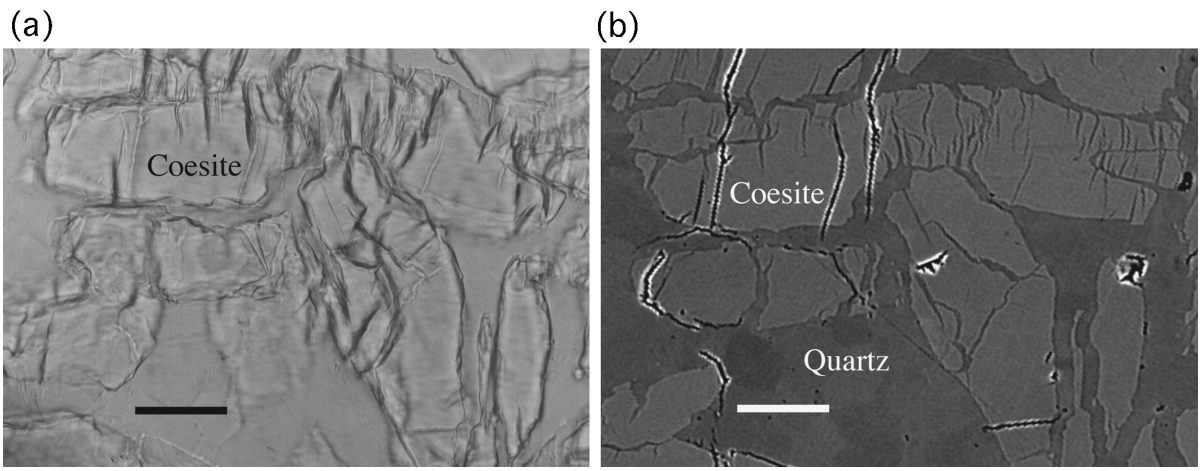

Fig. 4. a. Optical microphotograph (plane polarized light) showing cracks in coesite and interfaces between coesite and quartz. The scalloped, irregular shape of the interfaces suggests that nucleation was incoherent or semi-coherent.
b. BSE image of same area. Note distinction between cracks formed during decompression and/or sample preparation (*black*) and fractures in coesite filled with quartz (*dark gray*), which are inferred to have formed at high pressure. Some coesite does not appear in the BSE image because it does not intersect the surface of the thin section, even though it appears in focus optically. *Scale bars* = 50 μm.

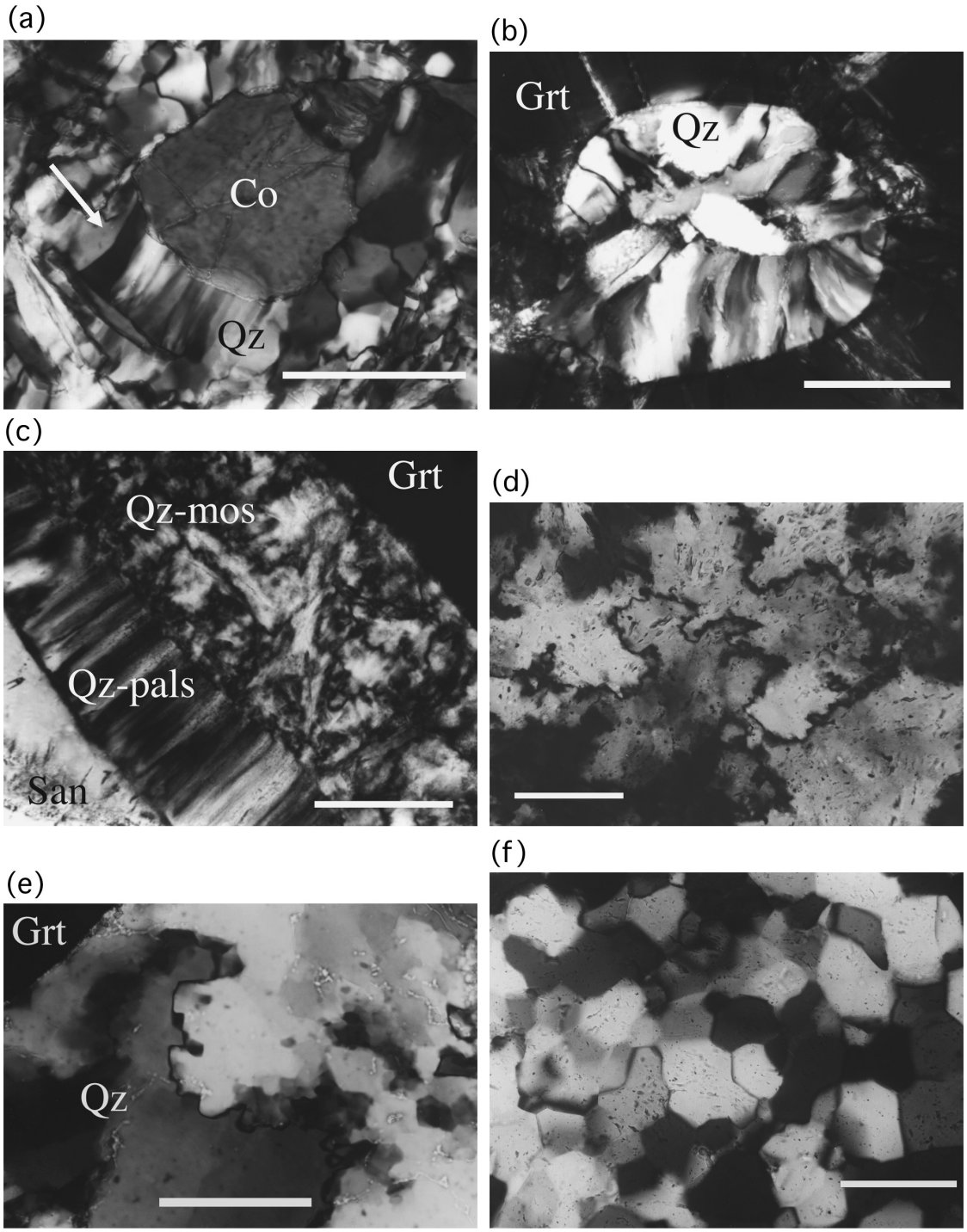
(a)
Co
Qz
(b)
Grt
Qz
(c)
Grt
Qz-mos
Qz-pals
San
(d)
(e)
Grt
Qz
(f)

3. Transformation textures and reaction mechanism

The evolution of reaction textures was observed by examining experiments of different durations as well as the variation of texture across the temperature gradient in individual samples. In the first stage of transformation, quartz nucleates and grows on coesite grain boundaries. After ~30–40% transformation, cracks commonly develop in the coesite crystals, providing new sites for nucleation and growth of quartz (Fig. 4). The existence of quartz in the cracks and the lack of cracks in untransformed samples strongly suggest that these features form at high pressure rather than during decompression. This is surprising because it is commonly considered impossible for fractures to be held open at such high pressures under nominally dry conditions. One possibility is that they are shear (mode II) cracks with no open volume [23]. Similar quartz-filled cracks are very commonly found in natural coesite inclusions, although they probably form at much lower pressures coincident with fracturing of the host phase (see below, Section 5.1).

In early to intermediate stages of transformation, the quartz crystals are typically elongate, with their long axes perpendicular to the host coesite grain boundary (Fig. 5a). This growth pattern is virtually identical to the ''palisade'' texture common in natural coesite pseudomorphs, where coesite grain margins have transformed to a radially disposed aggregate of quartz crystals grown perpendicular to the interface with the host phase (Fig. 5b and c). More rarely, palisade quartz is preserved outside of inclusions in the groundmass of rocks; the best examples are from Dora Maira pyrope quartzites [24]. Universal-stage measurements [4] and electron diffraction [6] have revealed no systematic crystallographic relationship (epitaxy) between the palisades and their substrate in natural rocks; similar textures in our experiments also suggest lack of epitaxy, but we have not yet demonstrated this conclusively.

With increasing duration of the experiments, the palisades are replaced by a ''mosaic'' texture composed of quartz grains sutured by highly dentate, high-angle boundaries (Fig. 5d). Each grain contains tens to hundreds of subgrains of similar orientation. This texture has also been seen in inclusions of partially transformed coesite and coesite pseudomorphs in natural rocks[25–27] and in a grospydite xenolith from the Roberts Victor Mine (Fig. 5c; [28]). Furthermore, we have identified a very similar texture in the groundmass of a coesite-bearing, quartz-rich eclogite from the Dabie Shan (Fig. 5e).

Recrystallization of the mosaic texture leads progressively to a polygonal texture (Fig. 5f). We interpret the textural changes as evidence of progressive recovery and recrystallization driven by the transformation stress and resulting strain induced by the large volume change of the reaction. The observed textures, particularly the transition from mosaic to polygonal microstructure, indicate both subgrain rotation and grain boundary migration [29,30], but we have not assessed the relative importance of these two recrystallization mechanisms. We suggest that the observed microstructures are roughly analogous to those of the ''regime 3'' recrystallization regime delineated by Hirth and Tullis [30] on the basis of

Fig. 5. Comparison of synthetic and natural reaction textures. All microphotographs taken in cross-polarized light, *scale bars* = 100 μm.
a. Palisade quartz (*arrow*) in sample transformed at 850°C, 200 MPa understep, for 120 h (#364).
b. Palisade quartz pseudomorph of coesite inclusion in garnet in pyrope quartzite from the Dora Maira massif.
c. Palisades in a coesite pseudomorph in a grospydite xenolith from the Roberts Victor Mine [28]. Part of the pseudomorph exhibits a mosaic texture (*Qz-mos*) similar to textures shown in (d) and (e).
d. Synthetic mosaic structure, showing high-angle, serrated grain boundaries between quartz grains containing several subgrains. Similar boundaries are found in earlier stages of transformation where opposing sets of palisade crystals have converged. Sample transformed at 800°C, 400 MPa understep, for 96 h (#369).
e. Mosaic texture in quartz groundmass in a quartz-rich eclogite from the Dabie Shan (#62B). Note high-angle grain boundary similar to those in (d). The same thin section contains coesite inclusions exhibiting a similar texture in garnet, kyanite and omphacite. This suggests that the texture is related to the transformation, although we cannot preclude the possibility that it is instead related to deformation not associated with the transformation.
f. Polygonal texture achieved after 144 h at 900°C, 200 MPa understep (#302). The large grain size of this sample compared to that in (d) is a result of grain growth in addition to subgrain rotation.

deformation experiments on quartzite. However, the experimental samples are distinguished by the lack of a ''core and mantle'' microstructure, typical of their regime 3.

The transformation stress causes brittle failure of coesite at conditions under which quartz deforms plastically [30], supporting previous suggestions that coesite is stronger than quartz [6]. A similar contrast in response to transformation stress has been observed for the aragonite $\rightleftharpoons$ calcite transformations [14,31,32], although the experiments in these studies were unconfined. The clear evidence for transformation strain and subsequent stress relaxation has important implications for the kinetics of the transformation, as discussed below.

4. Kinetic data

4.1. Growth rates

Growth rates were determined by measuring the length of the longest palisade quartz crystal in thin section, and dividing that number by two and the duration of the experiment. Use of this technique relies on the following assumptions: (1) nucleation was instantaneous; (2) the longest crystal represents the first nucleated; (3) no impingement by other quartz grains has occurred; (4) the shape of the original quartz crystals has not been modified by subsequent recrystallization; (5) the quartz grew equally fast in two directions; and (6) the growth rate was constant.

The assumption of instantaneous nucleation appears to be reasonable, at least for the higher-temperature experiments, because the shape of the ξ–t curves (see below) does not give any indication of an incubation period for the transformation. The second consideration above is the best assumption that can be made when nucleation and growth have not been observed in situ, but may lead to an uncertainty due to geometrical sampling error. Assumptions (3) and (4) can also be justified for growth rates that were measured in samples exhibiting early stages of transformation, for which textural observations indicate that no impingement or recrystallization has occurred. The last two assumptions, however, are the most difficult to assess and could lead to significant error in determination of the activation energy for growth. Assumption (5) may be a reasonable approximation if the interfaces with the host coesite on either side of the growing crystal were similar, yielding the same resistance to growth. This would not be the case if the quartz shared a less mobile, coherent interface with one of the host coesite crystals [33]. However, as discussed above, existing textural observations lend no support for an epitaxial relationship between the two phases.

The common assumption (6) of constant growth rate during polymorphic phase transformations has been questioned by two recent studies, in which growth slowed drastically or stopped completely after an initial period of linear growth. In the first study, the growth of calcite crystals in single-crystal aragonite slowed after the aragonite fractured, and stopped completely after the calcite crystals reached a critical size [14]. Cessation of growth was also reported for β and γ phases of $Mg_{1.8}Fe_{0.2}SiO_4$

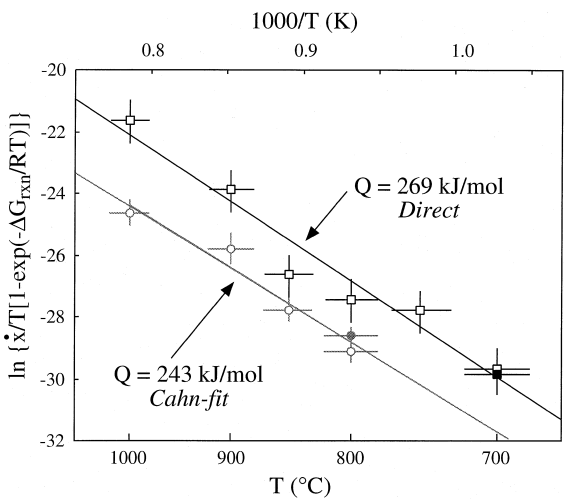

Fig. 6. Arrhenius diagram showing the temperature dependence of measured and extrapolated growth rates ($\dot{x}$), normalized to account for the magnitude of reaction free energy (ΔG_{rxn}) [11]. *Circles* are growth rates extrapolated by fitting the Cahn equation (see text); *squares* are directly measured growth rates. *Open symbols*: 190–220 MPa understep; *closed symbols*: 400–410 MPa understep. Uncertainties for measured growth rates represent 30% uncertainty in length measurement and $\pm$20°C in temperature. Uncertainties in the growth rates determined by fitting the Cahn equation were assessed by taking the uncertainties in ΔG_{rxn} and ξ into account. Weighted least-squares fits to the data give the activation energies shown.

growing into single crystals of San Carlos olivine from the grain boundary with a polycrystalline olivine matrix [34].

Liu and Yund [14] proposed loss of coherency between the two phases, following fracturing of the aragonite, as a cause for the decrease in growth rate. The development of transformation stress may be another important factor. Although the volume change of the reaction should theoretically be accommodated by relaxation of other components in the pressure cell, the efficiency of this process is not well understood. Therefore, grain-scale transformation stresses may induce a localized pressure change back toward equilibrium, resulting in a decrease in the driving force for growth [11]. Further growth would then be controlled by the rate of stress relaxation. We suspect that such a model may be applicable to the growth of quartz in our experiments, where high transformation stresses are clearly indicated by microstructural evidence. That growth does not stop completely in our experiments is probably related to the rapid recovery process in quartz at the high temperatures of the experiments.

Despite these uncertainties, we fit our growth rate data to Turnbull's equation for interface-controlled growth [35]:

$$\dot{x} = k_0 T\left[\exp(-Q/RT)\{1-\exp(-\Delta G/RT)\}\right] \quad (1)$$

where $\dot{x}$ = growth rate, k_0 = a constant; T = temperature, Q = activation energy for growth; R = the universal gas constant, and ΔG = the free energy change of the reaction, which was calculated using the thermodynamic data set of Holland and Powell [36] after adjusting the value for pressure according to the calibration. In order to avoid possible effects of impingement, recrystallization, or transformation stress, we only used growth rate data for the shortest experiments ($< 30\%$ ξ) in a given isobaric/isothermal series. Q (269 ± 26 kJ/mol) and k_0 (26.537) were determined from the slope and intercept, respectively, of a weighted least-squares linear fit to the growth rate data on an Arrhenius plot (Fig. 6).

4.2. Overall transformation kinetics

Data for the volume fraction transformed as a function of time were fit at several different temperatures using a modified form of the Avrami equation, derived by Cahn [37] to describe reactions characterized by grain boundary nucleation and growth:

$$\xi = 1 - \exp\left[-2S\int_0^{y'}\{1-\exp(-z)\,dy\}\right] \quad (2)$$

where

$$z = \pi\int_0^{t-t'}\dot{N}\left[\dot{x}^2(t-\tau)^2 - y^2\right]d\tau$$

and ξ = the volume fraction of product transformed, S = grain boundary area, $y' = \dot{x}t$ (the growth distance after time t), $\dot{N}$ = nucleation rate, τ = the time at which a nucleus forms, and t' is the time for a nucleus to grow to radius y. For tetrakaidecahedral grains, $S = 3.35/d$, where d = average grain size. We used this approximation for the coesite starting material even though the grains are not tetrakaidecahedra. Liu and Yund [14] used the same approximation for aragonite and found no significant difference in the determination of grain boundary area. The uncertainty induced by this simplification is thought to be small relative to the other uncertainties noted.

Eq. (2) was fitted to the experimental ξ–t data using a non-linear regression algorithm, with $\dot{N}$ and $\dot{x}$ used as fitting parameters in order to minimize a chi-square function [14,38]. The best fits, together with the optimized values for $\dot{N}$ and $\dot{x}$ and the chi-square ($\chi 2$) value, are shown in Fig. 7. In all cases, it was only possible to determine minimum values for $\dot{N}$, whereas the values for $\dot{x}$ were uniquely determined. The difficulty in determining $\dot{N}$ is largely caused by high rates of nucleation relative to growth under experimental conditions, leading to dominance of $\dot{x}$ in determining the shape of the curve [38].

The optimized growth rates were fitted to Eq. (1), as shown in Fig. 6. The activation energy calculated using this method (243 ± 19) is the same, within error, as that calculated from the direct measurements as discussed above. However, the value for k_0 (0.185) is substantially different, as belied by the systematic difference in growth rates (up to two orders of magnitude) estimated by the two methods. The reason for this discrepancy is not clear. It may be related to a decrease in growth rate caused by the

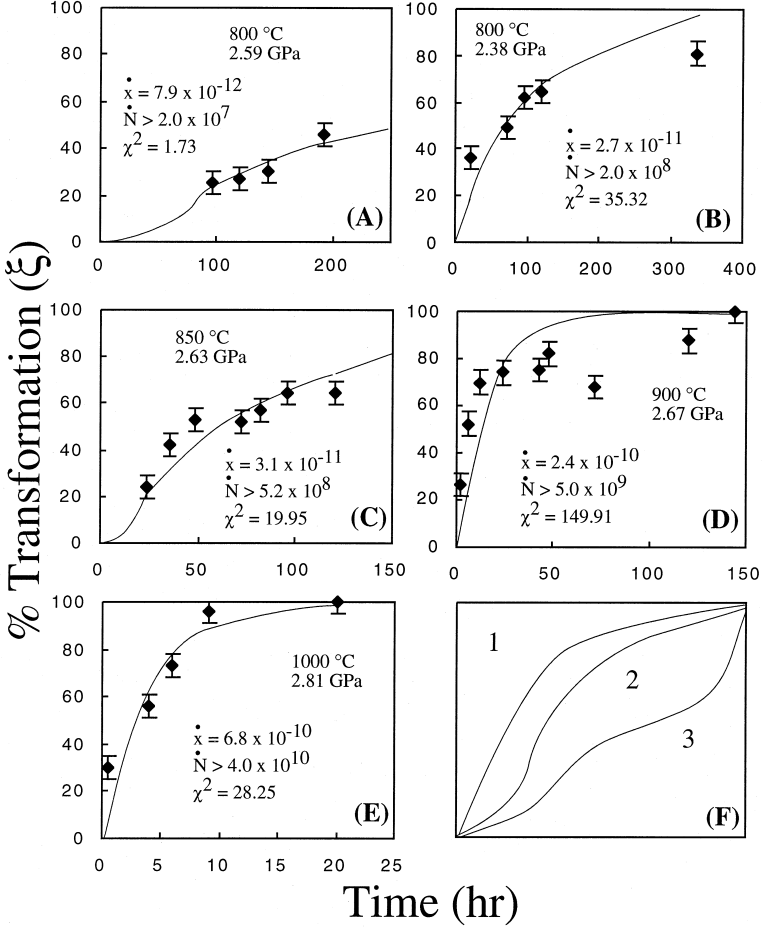

Fig. 7. (A)–(E). ξ–t curves obtained by fitting Eq. (2) to the kinetic data (*diamonds*) at labeled temperatures and pressures. Optimized values of $\dot{N}$ and $\dot{x}$ are shown together with the weighted chi-squared value (χ^2).
(F). Schematic diagram showing the theoretical shape of ξ–t curves. Curves *1* and *2* represent transformations conforming to classic Avrami theory; curve *1* results from high nucleation rate ($\dot{N}$) relative to growth rate ($\dot{x}$), while curve *2* represents the more general case in which transformation is controlled at first by the rate of nucleation. Curve *3* is a conceptual view of how transformation stress might affect the curve. Inhibition of growth by the transformation stress results in the curve leveling off at intermediate stages of transformation. Growth, at a much slower rate, is then controlled by the rate of stress relaxation. The rate may increase again following complete stress relaxation and/or the creation of new nucleation sites. The exact shape of the curve will likely be much more complex, depending on the rates of and interaction between stress relaxation, nucleation and growth.

transformation stress, as discussed above. Thus, because the Cahn equation was derived based on the fundamental assumption of constant, linear growth under isothermal, isobaric conditions, the model may be inappropriate. This may help to explain why fitting the Cahn equation to the data sometimes results in an overestimation of the actual ξ (e.g., Fig. 7C and E). However, this discrepancy may alternatively be caused by non-systematic pressure uncertainties between different experiments, as discussed in Section 2.1.

5. Implications for the preservation of coesite

The similarity between textures in our experimental charges and textures of natural coesite-to-quartz reaction in rocks from a wide variety of localities is

striking. This lends confidence that dominant reaction mechanisms are similar in both cases, which is a crucial prerequisite to meaningful extrapolation of laboratory reaction rates to geologic conditions. Constraints can be placed on the preservation of coesite in UHP rocks by extrapolating growth rates to lower temperatures and making some assumptions about nucleation. As an approximation, we extrapolated transformation rates assuming instantaneous nucleation. This simplistic assumption is probably justified, considering that reaction in nature can take place during decompression at large understeps (up to ~ 2.5 GPa) of the equilibrium boundary.

If instantaneous nucleation is assumed, a simplified form of Cahn's equation can be used, representing interface-controlled growth following saturation of nucleation sites [37]:

$$\xi = 1 - \exp\left[-2 S_g \dot{x} t\right]$$

where S_g = grain boundary area, $\dot{x}$ = growth rate, and t = time. This equation was solved to determine the P–T–t conditions necessary to completely transform coesite of a given grain size, using growth rates calculated from Eq. (1) and employing two sets of parameters obtained by the two different methods described above (Sections 4.1 and 4.2). It must be emphasized that the results, shown in Fig. 8, are only reasonable for large deviations from equilibrium, under which nucleation is considered to be rapid. The shape of the curves close to equilibrium is thus subject to the most uncertainty, but a more accurate representation cannot be given at this time due to poor constraints on nucleation rates.

For times in the range of 0.1–100 m.y., extrapolation using either set of growth rate parameters yields nearly identical results. Fig. 8 indicates that coesite crystals on the order of 100 μm in diameter will be completely consumed at temperatures $\gtrsim 375$°C in ≤ 1 m.y. This result must be reconciled with the fact that coesite is preserved in rocks known to have decompressed into the quartz stability field at temperatures as high as granulite-facies conditions [39]. In the absence of other factors, therefore, our data indicate that unreasonably fast exhumation rates would be required for preservation.

How can the discrepancy between the experimental results and natural evidence be reconciled? Below we consider the following possible factors: (1) inclusion of coesite in a strong host phase, such as garnet; (2) the influence of transformation stress; and (3) the effect of fluids.

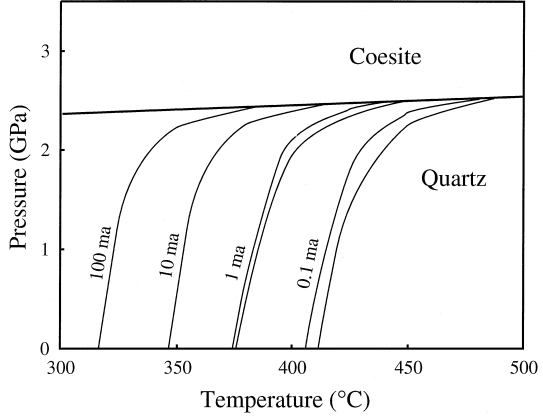

Fig. 8. Extrapolated times required for 100% conversion of coesite to quartz, for a grain size of 100 μm. All curves were calculated relative to the equilibrium boundary of Bohlen and Boettcher [41]. The *solid curves* were calculated using the growth parameters obtained from fitting the Cahn equation, while the *dashed curves* were calculated using the parameters obtained by fitting the directly measured growth rates. Increasing the grain size by an order of magnitude has the same effect as decreasing the time by an order of magnitude, i.e. the curves shift upwards in temperature by ~ 25°C.

5.1. Elastic inclusion models

Two nearly identical models have been developed to explain the preservation of coesite inclusions in garnet based on the elastic properties of the phases [7,40]. According to the models, the host phase exerts an overpressure on the inclusion, constraining its P–T path to the quartz–coesite equilibrium boundary. Small increments of reaction, as permitted by the thermoelastic response of the phases to changes in P and T, then buffer the pressure on the coesite back to the equilibrium value. The predictions of both studies are essentially identical: on a P–T path typified by that depicted in Fig. 9, 25–30% transformation can occur prior to fracturing of the host, which occurs at low temperature (~ 400°C) when the inclusion pressure exceeds three times the outside pressure [7]. Under these conditions, the remaining coesite is presumed to be preserved because of slow reaction kinetics [40], inferred from the sluggishness of the transformation at low temperatures and laboratory time scales in phase equilibria

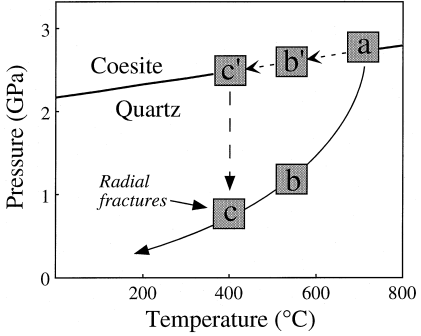

Fig. 9. Model for retention of coesite included in garnet, adapted after [40,7]. The rock experiences a $P-T-t$ path (based on a path inferred for the Dora Maira massif) from UHP metamorphism (a) through a greenschist-facies overprint (b). The inclusion follows a path along the equilibrium boundary ($a-b'$), due to the overpressure exerted by the host phase. During this time, $\sim 25-30\%$ quartz can form, as constrained by the compressibility and thermal expansivity of the phases. When the inclusion pressure ($c' = 2.4$ GPa) reaches three times that of the external pressure ($c = 0.8$ GPa), fracturing of the host occurs, allowing transformation to proceed normally along the remainder of the $P-T-t$ path.

studies [41]. However, extrapolation of our kinetic data suggests that transformation will be very rapid (complete in < 1 m.y.) at such conditions. This underscores the need for reassessment of the elastic models.

Constraining the pressure of the inclusion to the quartz–coesite equilibrium boundary assumes that reaction along the boundary is instantaneous, effecting an instantaneous volume change. In reality, even at relatively high temperatures, reaction close to the boundary may be inhibited by slow nucleation kinetics. Thus, the inclusion pressure could deviate significantly from the equilibrium curve before reaction occurs, buffering pressure back to equilibrium and resulting in less transformation than that predicted by the model. Ultimately, however, it seems unlikely that nucleation would be suppressed along a $P-T$ path at deviations as much as 1.5 GPa from the equilibrium boundary, at which point cracking of the host phase occurs. If any nuclei form during decompression prior to fracture of the host, the high growth rates inferred from this study will result in total consumption of the inclusion. This suggests that an additional mechanism is required to preserve coesite.

Recently, intergranular coesite crystals were discovered in regional UHP metamorphic rocks from the Sulu region in China [42]. Because these grains share interfaces with two or more other phases, their preservation cannot be explained by the elastic inclusion models. It is conceivable that the transformation can be affected by the flow strength of adjacent phases even though the coesite is not surrounded by a single strong mineral. A more likely explanation entails restricted fluid infiltration, as discussed in Section 5.3.

5.2. Transformation stress

Transformation stress and strain can affect both growth and nucleation rates [14,43,44], although details of the interaction are not quantitatively well understood. Elastic strain energy inhibits nucleation, with especially dramatic effects at low temperatures where the magnitude of the strain energy can approach that of the chemical free energy of the transformation [14,44]. The effect has only been modeled for the relatively simple case of homogeneous, intragranular nucleation [44,45]. The effect of elastic strain energy on heterogeneous nucleation on grain boundaries is expected to be reduced by permanent (plastic) deformation of the phases, but the amount of reduction is difficult to constrain [14]. Natural microstructures in quartz pseudomorphs after coesite indicate that permanent deformation has indeed played a role in the transformation, as demonstrated above. As a further complication, highly strained regions of the host may serve as *enhanced* sites for nucleation [11]. Textural evidence from our experiments suggests that cracks which form at high pressure in coesite serve as new nucleation sites.

Of perhaps greater concern for the coesite → quartz transformation is the unconstrained effect of elastic strain energy on growth rates, as discussed previously. At present it is difficult to model quantitatively the effect at lower temperatures appropriate for extrapolation. If a decrease in growth rates occurs because of transformation stress, the rate of the reaction may ultimately be controlled by the rate of stress relaxation, which depends not only on temperature but to a large extent the amount of H_2O present, considered in the next section.

5.3. The effect of fluids

Fluids are well known to have a catalytic effect on reactions, although the dependence of kinetics on

fluid concentration and the precise mechanisms of catalysis are still poorly constrained [46]. One mechanism that may be important, if stress relaxation plays a role in controlling reaction rates, is the ''hydrolytic weakening effect'' of trace amounts of H_2O. Although hydrolytic weakening has not been demonstrated for coesite, it must promote the relaxation of elastic strain energy in quartz, affecting reaction as discussed above. H_2O also increases the diffusion rate of oxygen in silicates [47] and may affect the diffusion rate of other ions. Furthermore, by reducing the activation energy required to break Si–O bonds, fluids may enhance nucleation. To date, few studies have specifically examined the effect of trace volatiles on phase transformations or even characterized the fluid content of the starting material (for an exception, see [48]).

One possibility is that the H_2O content in our experimental samples is higher than that which was available to promote reaction in partially preserved coesite in nature, which could explain the discrepancy between the extrapolation and the natural evidence. This hypothesis is indirectly supported by a number of observations from UHP rocks, including the finding of intergranular coesite [42] and the preservation of primary igneous textures and mineralogy in eclogites [49]. Evidence for restricted fluid flux during metamorphism and exhumation is also provided by record-low $\delta^{18}O$ values in UHP eclogites, which indicate a lack of re-equilibration under high P–T conditions [50]. Furthermore, direct measurements by FTIR failed to detect any OH defects or molecular H_2O in coesite from the Roberts Victor Mine xenolith [51], suggesting that natural coesite, unlike quartz, may not incorporate significant H_2O. Further experiments with different fluid contents, in tandem with investigations of natural UHP rocks using fluid inclusion microscopy, FTIR and oxygen isotopes, are thus needed to assess the effect of small amounts of aqueous fluid on kinetics.

6. Conclusions

This study represents one of the first conclusive demonstrations that natural reaction mechanisms of solid–solid metamorphic reactions can be duplicated in the laboratory. Although this is a crucial prerequisite for extrapolation of experimental data to natural conditions, the extrapolation is complicated by a number of factors in need of further investigation. The disparity between growth rates calculated by direct measurements and by extrapolation using Cahn's modification of the Avrami equation is disturbing in that fits to both sets of data show excellent correlations with temperature. This may be due to a systematic error in the direct measurements. On the other hand, the use of Cahn's formulation for extrapolating growth and nucleation rate parameters from kinetic data may suffer from a significant uncertainty because of the unconstrained effect of transformation stress on growth rates, which has not been taken into account by previous studies on mineral reactions [14,38,52]. This underscores the need for more quantitative modeling of the interaction between elastic strain energy, plastic relaxation processes, and reaction kinetics in systems involving heterogeneous grain-boundary nucleation and growth. In addition, evidence from natural rocks, as well as experimental data on the solubility of OH in nominally anhydrous minerals [53], suggest that the role of trace fluids in promoting kinetics needs to be evaluated quantitatively. Further study of these effects will have ramifications not only for the exhumation of deeply subducted continental rocks, but for the kinetics of phase transformations elsewhere in the Earth.

Acknowledgements

We thank W.B. Hankins for laboratory assistance, T.N. Tingle and R.E. Jones for help with digital image acquisition, D.C. Rubie for discussions, and P.J. O'Brien, J.G. Liou, and J.R. Smyth, for donations of natural samples. The manuscript was improved by thoughtful and comprehensive reviews from P. Burnley, W.G. Ernst, P. Gillet, B.R. Hacker, and M. Liu. Support for this research was provided by the U.S. Geological Survey, the Mineralogy and Petrology Research Award from the Mineralogical Society of America (to JLM), and grants from the Geological Society of America and the McGee and Shell Funds of Stanford University to JLM. This paper is dedicated to T.N. Tingle. *[FA]*

References

[1] R.G. Coleman, X. Wang, Ultrahigh Pressure Metamorphism, Cambridge University Press, Cambridge, 1995, 528 pp.

[2] L. Dobrzhinetskaya, H.W. Green II, S. Wang, Alpe Arami: a peridotite massif from depths of more than 300 kilometers, Science 271 (1996) 1841–1844.

[3] J.P. Platt, Exhumation of high-pressure rocks: a review of concepts and processes, Terra Nova 5 (1993) 119–133.

[4] B.R. Hacker, S.M. Peacock, Creation, preservation and exhumation of UHPM rocks, in: R.G. Coleman, X. Wang (Eds.), Ultrahigh Pressure Metamorphism, Cambridge University Press, Cambridge, 1995, pp. 159–181.

[5] A. Hynes, J. Arkani-Hamed, R. Greiling, Subduction of continental margins and the uplift of high-pressure metamorphic rocks, Earth Planet. Sci. Lett. 140 (1996) 13–25.

[6] J. Ingrin, P. Gillet, TEM investigation of the crystal microstructures in a quartz–coesite assemblage of the Western Alps, Phys. Chem. Miner. 13 (1986) 325–330.

[7] I. Van der Molen, H.L.M. Van Roermund, The pressure path of solid inclusions in minerals: the retention of coesite inclusions during uplift, Lithos 19 (1986) 317–324.

[8] P. Monie, C. Chopin, $^{40}Ar/^{39}Ar$ dating in coesite-bearing and associated units of the Dora Maira massif, western Alps, Eur. J. Miner. 3 (1991) 239–262.

[9] B.R. Hacker, Q. Wang, Ar/Ar geochronology of ultrahigh-pressure metamorphism in central China, Tectonics 14 (4) (1995) 994–1006.

[10] J.L. Mosenfelder, S.R. Bohlen, W.B. Hankins, New method for making synthetic ''rocks'' for use in phase transformation studies, and initial results on the quartz ⇌ coesite transformations, Abstr. Prog., Geol. Soc. Am. 26 (7) (1994) 260.

[11] D.C. Rubie, A.B. Thompson, Kinetics of metamorphic reactions at elevated temperatures and pressures: an appraisal of experimental data, in: A.B. Thompson, D.C. Rubie (Eds.), Metamorphic Reactions: Kinetics, Textures, and Deformation, Springer, New York, 1985.

[12] J.E. Shelby, J. Vitko Jr., R.E. Benner, Quantitative determination of the hydroxyl content of vitreous silica, J. Am. Ceram. Soc. 65 (1982) C59–C60.

[13] M. Paterson, The determination of hydroxyl by infrared absorption in quartz, silicate glasses and similar materials, Bull. Minéral. 105 (1982) 20–29.

[14] M. Liu, R.A. Yund, Transformation kinetics of polycrystalline aragonite to calcite: new experimental data, modeling, and implications, Contrib. Mineral. Petrol. 114 (1993) 465–478.

[15] S.R. Bohlen, Equilibria for precise pressure calibration and a frictionless furnace assembly for the piston–cylinder apparatus, Neues Jahrb. Mineral., Monatsh. 1984 (9) (1984) 404–412.

[16] J.R. Farver, R.A. Yund, Grain boundary diffusion of oxygen, potassium and calcium in natural and hot-pressed feldspar aggregates, Contrib. Mineral. Petrol. 118 (1995) 340–355.

[17] J.M. Edmond, M.S. Paterson, Strength of solid pressure media and implications for high pressure apparatus, Contrib. Mineral. Petrol. 30 (1971) 141–160.

[18] T.N. Tingle, Retrieval of uncracked single crystals from high pressure in piston–cylinder apparatus, Am. Mineral. 73 (1988) 1195–1197.

[19] J.L. Mosenfelder, S.R. Bohlen, W.B. Hankins, ''The quartz–coesite transition revisited'', revisited, Am. Mineral. (submitted).

[20] K. Bose, J. Ganguly, Quartz–coesite transition revisited: reversed experimental determination at 500–1200°C and retrieved thermochemical properties, Am. Mineral. 80 (1995) 231–238.

[21] P.W. Mirwald, I.C. Getting, G.C. Kennedy, Low-friction cell for piston–cylinder high-pressure apparatus, J. Geophys. Res. 80 (1975) 1519–1525.

[22] W. Johannes, Pressure comparing experiments with NaCl, AgCl, talc, and pyrophyllite assemblies in a piston cylinder apparatus, Neues Jahrb. Mineral., Monatsh. 2 (1978) 84–92.

[23] G. Hirth, J. Tullis, The brittle–plastic transition in experimentally deformed quartz aggregates, J. Geophys. Res. 99 (1994) 11731–11747.

[24] C. Chopin, C. Henry, A. Michard, Geology and petrology of the coesite-bearing terrain, Dora Maira massif, Western Alps, Eur. J. Miner. 3 (1991) 263–291.

[25] M. Enami, Q. Zang, Quartz pseudomorphs after coesite in eclogites from Shandong province, east China, Am. Mineral. 75 (1990) 381–386.

[26] T. Reinecke, Very-high-pressure metamorphism and uplift of coesite-bearing metasediments from the Zermatt–Sass zone, Western Alps, Eur. J. Miner. 3 (1991) 7–17.

[27] E. Schmädicke, Quartz pseudomorphs after coesite in eclogites from the Saxonian Erzegebirge, Eur. J. Miner. 3 (1991) 231–238.

[28] J.R. Smyth, Quartz pseudomorphs after coesite, Am. Mineral. 62 (1977) 828–830.

[29] M.R. Drury, J. Urai, Deformation-related recrystallization processes, Tectonophysics 172 (1990) 235–253.

[30] G. Hirth, J. Tullis, Dislocation creep regimes in quartz aggregates, J. Struct. Geol. 14 (1992) 145–159.

[31] W.D. Carlson, Aragonite–calcite nucleation kinetics: an application and extension of Avrami transformation theory, J. Geol. 91 (1983) 57–71.

[32] P. Gillet, Y. Gerard, C. Willaime, The calcite–aragonite transition: mechanism and microstructures induced by the transformation stress and strain, Bull. Minéral. 110 (1987) 481–496.

[33] D.A. Porter, K.E. Easterling, Phase Transformations in Metals and Alloys, Chapman and Hall, London, 1982, 514 pp. (see especially p.279).

[34] L. Kerschhofer, T.G. Sharp, D.C. Rubie, Intracrystalline transformation of olivine to wadsleyite and ringwoodite under subduction zone conditions, Science 274 (1996) 79–81.

[35] D. Turnbull, Phase changes, Solid State Phys. 3 (1956) 225–306.

[36] T.J.B. Holland, R. Powell, An enlarged and updated internally consistent thermodynamic dataset with uncertainties and correlations: the system K_2O–Na_2O–CaO–MgO–MnO–FeO–Fe_2O_3–Al_2O_3–TiO_2–SiO_2–C–H_2–O_2, J. Metam. Geol. 8 (1990) 89–124.

[37] J.W. Cahn, The kinetics of grain boundary nucleated reactions, Acta Metall. 4 (1956) 449–459.
[38] D.C. Rubie, Y. Tsuchida, T. Yagi, W. Utsumi, Kikegawa, O. Shimomura, A.J. Brearley, An in situ X-ray diffraction study of the kinetics of the Ni_2SiO_4 olivine–spinel transformation, J. Geophys. Res. 95 (1990) 15829–15844.
[39] Q. Wang, A. Ishiwatari, Z. Zhongyan, T. Hirajima, N. Hiramitsu, M. Enami, M. Zhai, J. Li, B. Cong, Coesite-bearing granulite retrograded from eclogite in Weihai, eastern China, Eur. J. Miner. 5 (1993) 141–152.
[40] P. Gillet, J. Ingrin, C. Chopin, Coesite in subducted continental crust: $P-T$ history deduced from an elastic model, Earth Planet. Sci. Lett. 70 (1984) 426–436.
[41] S.R. Bohlen, A.L. Boettcher, The quartz–coesite transformation: a precise determination and the effects of other components, J. Geophys. Res. 87 (1982) 7073–7078.
[42] J.G. Liou, R.Y. Zhang, Occurrences of intergranular coesite in ultrahigh-*P* rocks from the Sulu region, eastern China: implications for lack of fluid during exhumation, Am. Mineral. 81 (1996) 1217–1221.
[43] K. Honda, M. Sato, On the theory of transformation stress, in: Reactivity of Solids, Proc. 2nd Int. Symp. on the Reactivity of Solids, Gothenburg, 1954, pp. 847–857.
[44] M. Liu, R.A. Yund, The elastic strain energy associated with the olivine–spinel transformation and its implications, Phys. Earth Planet. Inter. 89 (1995) 177–197.
[45] J.K. Lee, Y.Y. Earmme, H.I. Aaronson, K.C. Russell, Plastic relaxation of the transformation strain energy of a misfitting spherical precipitate: ideal plastic behavior, Metall. Trans. A 11A (1980) 1837–1847.
[46] D.C. Rubie, The catalysis of mineral reactions by water and restrictions on the presence of aqueous fluid during metamorphism, Mineral. Mag. 50 (1986) 399–415.
[47] S.C. Elphick, C.M. Graham, The effect of hydrogen on oxygen diffusion in quartz: evidence for fast proton transients?, Nature (London) 335 (1988) 243–245.
[48] T.E. Young, H.W. Green II, A.M. Hofmeister, D. Walker, Infrared spectroscopic investigation of hydroxyl in β-$(Mg,Fe)_2SiO_4$ and coexisting olivine: implications for mantle evolution and dynamics, Phys. Chem. Miner. 19 (1993) 409–422.
[49] R.Y. Zhang, J.G. Liou, Partial transformation of gabbro to coesite-bearing eclogite from Yangkou, the Sulu terrane, East China, J. Metam. Geol. 15 (1997) 183–202.
[50] T.-F. Yui, D. Rumble III, C.-H. Lo, Unusually low $\delta^{18}O$ ultra-high-pressure metamorphic rocks from the Sulu Terrain, eastern China, Geochim. Cosmochim. Acta 59 (13) (1995) 2859–2864.
[51] G.R. Rossman, J.R. Smyth, Hydroxyl contents of accessory minerals in mantle eclogites and related rocks, Am. Mineral. 75 (1990) 775–780.
[52] D.C. Rubie, C.R. Ross II, Kinetics of the olivine–spinel transformation in subducting lithosphere: experimental constraints and implications for deep slab processes, Phys. Earth Planet. Inter. 86 (1994) 223–241.
[53] D.R. Bell, G.R. Rossman, Water in the Earth's mantle: the role of nominally anhydrous minerals, Science 255 (1992) 1391–1397.